Atmos. Chem. Phys. Discuss., 10, 24563–24593, 2010
www.atmos-chem-phys-discuss.net/10/24563/2010/
doi:10.5194/acpd-10-24563-2010

Atmospheric Chemistry and Physics Discussions

Continuous isotopic composition measurements of tropospheric CO_2 at Jungfraujoch (3580 m a.s.l.), Switzerland: real-time observation of regional pollution events

B. Tuzson, S. Henne, D. Brunner, M. Steinbacher, J. Mohn, B. Buchmann, and L. Emmenegger

Empa, Swiss Federal Laboratories for Materials Science and Technology, Laboratory for Air Pollution and Environmental Technology, Überlandstr. 129, 8600 Dübendorf, Switzerland

Received: 27 September 2010 – Accepted: 11 October 2010 – Published: 20 October 2010

Correspondence to: B. Tuzson (bela.tuzson@empa.ch)

Published by Copernicus Publications on behalf of the European Geosciences Union.

Abstract

A quantum cascade laser based absorption spectrometer (QCLAS) is applied for the first time to perform in situ, continuous and high precision isotope ratio measurements of CO_2 in the free troposphere. Time series of the three main CO_2 isotopologue mixing ratios ($^{12}C^{16}O_2$, $^{13}C^{16}O_2$ and $^{12}C^{18}O^{16}O$) have simultaneously been measured at one second time resolution over two years (from August 2008 to present) at the High Altitude Research Station Jungfraujoch (3580 m a.s.l., Switzerland). This work focuses on periods in February 2009 only, when sudden and pronounced enhancements in the tropospheric CO_2 were observed. These short-term changes were closely correlated with variations in CO mixing ratios measured at the same site, indicating combustion related emissions as potential source. The analytical precision of 0.046‰ (at 50 s integration time) for both $\delta^{13}C$ and $\delta^{18}O$ and the high temporal resolution allowed the application of the Keeling plot method for source signature identification. The spatial origin of these CO_2 emission sources was then determined by backward Lagrangian particle dispersion simulations.

1 Introduction

The accentuated mixing ratio increase of carbon dioxide (CO_2) and other trace gases in the Earth's atmosphere related to human activities is of major concern for climate change, because these anthropogenic emissions are gaining a significant role as an additional external forcing factor (Andres et al., 1999). Currently, CO_2 resulting from the burning of fossil fuel (6 GtC yr^{-1}) represents the single largest perturbation to the atmospheric budget on an annual basis for total carbon. However, accounting for the fate of this anthropogenic CO_2 in every detail is still very challenging (Archer et al., 2009), because of the complexity and variability of the global cycles in which CO_2 is involved (Tans et al., 1989; Conway et al., 1994; Francey et al., 1995; Keeling et al., 1995; Randerson et al., 1997). Stable isotopic composition measurement of atmospheric CO_2

ACPD
10, 24563–24593, 2010

can provide additional and essential information about the various pathways and processes. The ^{13}C isotopic distribution for example, allows for partitioning between land and ocean uptake ($3\,GtC\,yr^{-1}$) (Ciais et al., 1995). This is due to the differences in isotopic discrimination against ^{13}C associated with C_3 terrestrial ecosystem photosynthesis/respiration (~ 19‰) and air-sea gas exchange (~ 2‰). Similarly, anthropogenic CO_2 originating mainly from fossil fuel burning has a distinguishable isotopic signature that can be used as a tracer to understand and identify the sources and their temporal and spatial variations (Pataki et al., 2003a).

Similarly, the oxygen isotope composition of atmospheric CO_2 was also shown to be a powerful tracer of photosynthetic and respiratory carbon fluxes, but its application to carbon cycle studies is challenging, as has been reported by several studies (Francey and Tans, 1987; Yakir and Wang, 1996; Ciais et al., 1997). The complexity of the $\delta^{18}O$ data interpretation is due to the presence of an additional exchange of oxygen isotopes of CO_2 with water in leaves and soils, that is, isotope exchange without concentration changes. This creates severe limitations to the simple two-end member assumptions associated with the Keeling plot method. On a global scale, the ^{18}O isotopic content of CO_2 is mainly determined by the isotopic signature of the equilibrating water, which itself undergoes strong seasonal and latitudinal variations (Francey and Tans, 1987; Ciais et al., 1997). Thus, the atmospheric CO_2 is getting enriched in ^{18}O by oxygen isotope exchange with ocean and leaf water, but depleted by exchange with soil water and by anthropogenic emission of CO_2 leading to a seasonal pattern with an amplitude of about 1.5‰ in the northern hemisphere (Ciais et al., 1997). It is generally assumed that the ^{18}O signature of the CO_2 produced in combustion processes is equal to that of the atmospheric oxygen (Kroopnick and Craig, 1972). A mean $\delta^{18}O$ value for all combustion-derived CO_2 of −17‰, is therefore considered in the recent carbon cycle isotope models (e.g., Ciais et al., 1997; Cuntz et al., 2003).

Here we demonstrate the feasibility of improving anthropogenic CO_2 source identification and characterization at large regional scales by using laser spectroscopy as on-line and in situ measurement technique. For this purpose, an instrument was

ACPD
10, 24563–24593, 2010

designed and developed to perform high precision isotope ratio measurement of both $\delta^{13}C$ and $\delta^{18}O$ of atmospheric CO_2 at ambient mixing ratio. This spectrometer has been continuously measuring atmospheric CO_2 and its isotopic composition in real-time at the high Alpine observatory on Jungfraujoch that allows intermittent sampling of free tropospheric background air and polluted boundary layer influenced air. This CO_2 time-series together with the isotopic composition at high temporal resolution provide essential information for identification and characterization of pollution events, as presented in the following sections.

2 Experimental

2.1 Measurement site

The high Alpine research station Jungfraujoch (JFJ) is located in the western Swiss Alps on a mountain saddle at an altitude of 3580 m a.s.l. (46°33′ N, 7°59′ E). Given its high elevation and year-round accessibility, the station is an excellent place for long-term observations of free tropospheric air. Furthermore, its central position within the European continent and its particular topographical condition offers the opportunity to investigate the transport of anthropogenic CO_2 from the highly industrialized surrounding regions to the free troposphere (Balzani Lööv et al., 2008; Forrer et al., 2000). Since JFJ is part of the Swiss National Air Pollution Monitoring Network (NABEL) and of the World Meteorological Organization Global Atmosphere Watch (WMO-GAW) programme, a large number of trace gases and aerosol parameters are routinely monitored providing additional information for data interpretation.

2.2 Spectrometer setup

A detailed description of the instrumental design and signal processing has already been presented elsewhere (Nelson et al., 2008; Tuzson et al., 2008) and its field capability was demonstrated in several campaigns (Tuzson et al., 2008; Zeeman et al.,

ACPD
10, 24563–24593, 2010

2009; Kammer et al., 2010). The spectrometer has a modular construction to provide easy transport and setup. The three main parts are: optical module, control electronics and an automated calibration unit. Briefly, a pulsed quantum cascade laser (QCL, Alpes Lasers, Switzerland) emitting at 2310 cm^{-1} is used as mid-infrared light source. The beam is, after collimation, split in two parts of equal intensities and coupled into a dual-multipass cell assembly. This dual-cell arrangement allows for simultaneous sample/reference gas measurements which, since the sample mixing ratios are continually referenced to the stable isotope ratios of the reference gas, significantly improves the accuracy of the isotope ratio determination. Furthermore, uncertainties in the spectral fitting procedure are considerably reduced by applying the spectral analysis to the ratio of the sample and reference spectra. The simultaneous quantification of the three main CO_2 isotopologues ($^{12}C^{16}O_2$, $^{13}C^{16}O_2$ and $^{12}C^{16}O^{18}O$) is done by a commercial software for spectral analysis and laser control (TDLWintel, Aerodyne Inc., USA). Employing thermoelectrically cooled infrared detectors (PVI-3TE-4.4, Vigo System, PL) and quasi-room temperature QCL, a completely cryogen-free operation is achieved, which facilitates unattended and long-term measurements.

The instrument performance in terms of detection limit and stability over time was characterized on the sampling site by applying the Allan variance technique (Werle et al., 1993). Mixing ratios of the individual CO_2 isotopologues were measured with one second time resolution from a compressed air cylinder over a one hour period. Short-term precision at one second was 0.29‰, for both ratios, and the associated Allan variance plots had a minimum at 50 s which corresponds to a relative precision of 0.046‰, for both $\delta^{13}C$ and $\delta^{18}O$. For integration times beyond 50 s, the Allan plot showed a horizontal level up to 120 s and then an increasing variance indicated the presence of "drift" noise.

2.3 Sampling system and calibration method

The sampling and calibration system is schematically illustrated in Fig. 1. Air samples were drawn from the NABEL stainless steel main inlet (i.d. 8 cm, total length 3.1 m)

ACPD
10, 24563–24593, 2010

where the air flow is maintained at 50 $m^3 h^{-1}$ and at a constant temperature of 10 °C. A heated and PTFE coated diaphragm vacuum pump (N036ST.26E, KNF, Germany) maintained a constant flow of 1 L min^{-1} through a 15 m stainless steel tubing (1/4 in), which conducted the air stream to the laser spectrometer. Afterwards, the air from the pump outlet was directed through a Nafion drier (PD-100T, Perma Pure, USA) to eliminate volumetric effects on mixing ratio determinations, as well as to avoid collisional broadening effects due to the water vapour (Tuzson et al., 2010). A pressure relief valve was added between the pump outlet and the Nafion drier to avoid pressure build-up in the sampling line during calibration. Furthermore, a 0.5 L buffer volume was inserted to minimize pressure fluctuations due to the pump's pulsation. The air was then passed across a temperature stabilization module, a 7 µm sintered metal filter and continuously drawn (0.4 L min^{-1}) through the multi-pass cell (sample side) at a pressure of 8 kPa by an oil free diaphragm vacuum pump (N920 series, KNF, Germany). The flow rates and pressures in both cells were adjusted and maintained stable by a combination of thermal mass flow controllers (Red-y Smart series, Vögtlin Instruments, Switzerland) and low-flow metering valves (SS-SS6M, Swagelok, USA) at the cell inlet and on the downstream side, respectively. The instrument's sampling system periodically switched between calibration gases and air sample. The measurement cycle was as follows: (1) standard Tank A (every 15 min); (2) standard Tank B (every two hours); (3) standard Tank C (every 12 h); (4) air sample. Each calibration gas was sampled for 300 s, except Tank A for which the sampling was set to 130 s. This cycling was applied to the sample cell only, while through the reference cell a continuous flow (0.08 L min^{-1}) of reference gas (Tank A) was maintained during the entire campaign.

The calibration gases used in this study were produced in our laboratory based on gravimetric and dynamic dilution methods. This process involved the mixing in various amounts of two pure CO_2 gases from distinctively different sources (marine carbonate and methane burning) and their consecutive dilution by synthetic air. Finally, these special air mixtures were analyzed in the IsoLab at the Max-Planck Institute for Biogeochemistry (MPI-BGC, Jena, Germany). Their exact carbon and oxygen

ACPD
10, 24563–24593, 2010

isotopic composition were determined by high precision isotope ratio mass spectrometer (IRMS) analysis and expressed as the relative difference of isotopic abundance ratio relative to the "Jena-Reference AirSet" (J-RAS) standard reference material (Ghosh and Brand, 2003). The absolute δ^{13}C and δ^{18}O value of the J-RAS is closely linked to the V-PDB (Vienna-PeeDee Belemnite) -scale and is used to serve as a primary scale anchor for CO_2-in-air measurements. The CO_2 mixing ratio of each tank was linked to the WMO mole fraction scale by gas chromatography (Agilent 6890 gas chromatograph equipped with a CO_2 converter and a flame ionisation detector).

The instrumental response was previously characterized in the laboratory by using six calibration gases with CO_2 mixing ratios spanning the range of 384–1970 ppm and having isotopic compositions δ^{13}C of −4 to −37‰ and δ^{18}O of −5 to −29‰, respectively. The linearity and potential accuracy of the instrument for isotope ratio measurements (δ^{13}C and δ^{18}O) has been estimated to ±0.06‰ (1σ standard deviation), while the precision and accuracy of the CO_2 mixing ratio values is better than ±0.03 ppm (after 50 s integration time corresponding to the Allan-variance minimum) and ±0.1 ppm, respectively.

2.4 Backward Lagrangian particle dispersion simulations

The Lagrangian particle dispersion model (LPDM) FLEXPART (Stohl et al., 2005) was used in backward mode (Seibert and Frank, 2004) to characterize the source regions of the sampled air masses. The model was driven by 3-hourly European Center for Medium-range Weather Forecast (ECMWF) fields by alternating analyses and forecasts at 1° × 1° × 90 levels resolution globally and at a higher resolution of 0.2° × 0.2° for a nested domain covering central Europe to better represent the Alpine topography. For every 3-h observation interval 50 000 "particles" were released from JFJ and traced back over 5 days. The particles were released at 3000 m a.s.l. which is a compromise between the real station altitude (3580 m a.s.l.) and the model surface height at JFJ (2010 m a.s.l.). LPDMs provide a much more comprehensive view of the air-mass history than single trajectory models as they account for the dispersion of a retro-plume by

ACPD
10, 24563–24593, 2010

turbulent motion and convection. For each simulation a "footprint" was computed, i.e. a map of the residence time of the particles within a layer of 100 m above ground. The footprint can be interpreted as a source sensitivity function (given in units of $s\,m^3\,kg^{-1}$ (Seibert and Frank, 2004)): emission sources at places of high/low residence times have a high/low potential to have contributed to the observation. Finally, footprints of selected pollution or background measurement episodes were combined into single footprints to describe the general air mass origin during these periods.

3 Results and discussion

The very small variations in the isotopic composition of atmospheric CO_2 make their detection a challenging task. A back of the envelope estimate of the expected isotopic signal variability can be made as follows: the background tropospheric air has an approximate CO_2 content of 390 ppm (Northern Hemisphere, winter period, 2009) with an isotopic composition of $\delta^{13}C = -8.4‰$ and $\delta^{18}O = -0.3‰$, respectively. Assuming an additional admix of 10 ppm anthropogenic CO_2 originating from fossil fuel burning with an average $\delta^{13}C$ of −28‰ and $\delta^{18}O$ of −17‰ and applying the simple two source mixing model, this admix will induce a decrease of 0.5‰ and 0.4‰ in the measured $\delta^{13}C$ and $\delta^{18}O$ values, respectively. These signals are about twice the instrumental precision at one second resolution and 10 times higher than the achievable detection limit. The ability to generate a large number of data points at the highest possible precision is obviously necessary to maximize the constraints on the retrieved $\delta^{13}C$ and $\delta^{18}O$ values. Random measurement errors can efficiently be compensated by averaging one second QCLAS measurements over, for example, 10 min periods.

An objective estimate of the analyzer's long-term stability and accuracy was obtained by considering the retrieved values of the second standard gas (Tank B) after the calibration procedure was applied. Figure 2 shows the corresponding CO_2 mixing ratio and $\delta^{18}O$ values (two minutes average) during a one month measurement period. The histogram plots indicate that the data ($n = 324$) are nearly normally distributed. A

ACPD
10, 24563–24593, 2010

Gaussian fit to the distributions suggests an accuracy of the two minute averaged CO_2 mixing ratios and $\delta^{18}O$ values of about 0.08 ppm and 0.09‰, respectively. Since this describes the statistical uncertainty of single values, repeated measurements lead to an even lower error of the mean. Similar results were obtained for $\delta^{13}C$.

The laser spectrometer was installed at the JFJ research station in August 2008 and has been continuously delivering data at one second time resolution with a data availability of more than 96%. For this study, the analysis period was limited to one winter month (February, 2009) for two reasons: (1) the biological activity (photosynthesis) is presumably negligible for this period, making the interpretation of the data more straightforward, and (2) within this period we captured several short-term pollution events associated with a variety of pronounced meteorological conditions including frontal lifting and south Foehn events. These events induced a pronounced increase ($\geqslant$ 10 ppm) in the measured CO_2 with a clearly detectable change in its isotopic composition. Moreover, these distinct meteorological conditions allowed to spatially attribute emissions from the European continent by using the Lagrangian backward calculations and determining the footprint of the air masses.

High resolution time series of CO_2 mixing ratio and the corresponding $\delta^{13}C$ and $\delta^{18}O$ values are shown in Fig. 3. The data points represent 10 min averages, which give a smooth curve for the CO_2 mixing ratio. Because the scatter of $\delta^{13}C$ and $\delta^{18}O$ values is much accentuated at the permil scale, an interpolation line using a smoothing spline algorithm (Igor Pro v6, Wavemetrics, Inc.) is added as visual aid. The standard deviation parameter required by the algorithm was estimated to 0.09 and 0.07‰ for $\delta^{13}C$ and $\delta^{18}O$, respectively from the variability of the background air considered to characterize the noise in the time series accurately enough, so that the smoothing factor can be kept at the nominal value of one, thus avoiding any further smoothing of the data.

Several marked increases in CO_2 mixing ratios can be identified which point at frequent upward transport of air masses from the polluted boundary layer to Junfraujoch in February 2009. These increases coincide with partly very low $\delta^{13}C$ and $\delta^{18}O$ values

ACPD
10, 24563–24593, 2010

suggesting enhanced contributions from fossil fuel burning. In the following, four pollution episodes with distinct isotope signatures labelled I–IV in Fig. 3, are considered for further analysis. The analysis will be supported by measurements of carbon monoxide (CO) and FLEXPART footprints to characterize the sources in terms of origin and chemical signatures.

3.1 CO as proxy for fossil fuel CO_2

Fossil fuel emissions are the largest contributor to the CO burden in the northern hemisphere (Duncan et al., 2007). Given the relatively long atmospheric residence time of CO in winter (several months), it can be used as a quantitative tracer for fossil fuel burning and hence for CO_2 emissions from regional combustion sources (Zondervan and Meijer, 1996; Gamnitzer et al., 2006; Turnbull et al., 2006; Levin and Karstens, 2007; Turnbull et al., 2010). Furthermore, the ratio between CO and CO_2 enhancements provides valuable information on the type of combustion since high ratios are indicative for poorly controlled, incomplete combustion processes. The mixing ratios of CO were measured continuously at the same site with a nondispersive infrared instrument (APMA-360, HORIBA Ltd.) (Zellweger et al., 2009). For all individual events mentioned above, CO correlated with CO_2 to a high degree ($r^2 > 0.9$) as shown in Figure 4. Here, the linear regressions were calculated using the total CO mixing ratio and the CO_2 above tropospheric background (ΔCO_2), the latter being calculated as the difference between observed and background concentration level and referred to as fossil-derived CO_2. The background level was determined using low-pass filtering of the data (one year record) converted from the time domain into the frequency domain by a fast Fourier transformation. In this approach, the contribution of respired CO_2 from the biosphere is accounted for in the background air as a seasonal effect. Hence, the y-intercept given by the regression in Fig. 4 should represent the CO mixing ratios of continental background air for the specific season. In fact, the average value of the investigated one month period corresponds to 0.127 ± 0.001 ppm CO, which is in excellent agreement with the CO mole fractions of free tropospheric air when trends and

ACPD
10, 24563–24593, 2010

seasonal variations are considered (e.g. see Fig. 6a in Zellweger et al. (2009)). The correlation found for all selected time periods is significant, with r^2 as high as 0.985, which is a clear indication that sudden and effective transport of anthropogenic pollution from distinct regions with well constrained CO:CO_2 emission ratios took place. Since the slope values of the regression are closely related to the combustion type and quality, their variability from event to event is reflecting the differences in the source regions. Tunnel measurements representing local traffic and transport on the Swiss highways report a vehicle weighted mean CO:CO_2 [ppm/ppm] ratio of 0.008(3) linked to diesel and gasoline vehicles (Vollmer et al., 2007), which is in good agreement with the observed CO:CO_2 ratio for events II, III and IV. Hence, in all these cases the CO:CO_2 ratio suggests a "pure" and high temperature combustion process of fossil fuel, close to that of road transportation. However, event I shows a much steeper slope that may be indicative for a substantial contribution of biomass or wood burning for which much larger ratios have been reported (Andreae and Merlet, 2001).

3.2 δ^{13}C and δ^{18}O as CO_2 source identifier

As outlined above, the stable isotope ratios $^{13}C/^{12}C$ and $^{18}O/^{16}O$ in the measured CO_2 are expected to contain information about the characteristics of the various pollution sources averaged over a regional scale. The pronounced short-term variations in CO_2 mixing ratio during the pollution events are well suited to utilize the Keeling plot method for deriving the isotopic composition of the pollution sources. In agreement with the simple mixing model developed by Keeling (Keeling, 1958), a plot of the measured $\delta^{13}C$ as a function of $1/[CO_2]$ gives a straight line relationship with the intercept representing the integrated measure of the isotopic composition of CO_2 emitted by a source ($\delta^{13}C_s$). To obtain sufficiently precise y-intercept values, the Keeling plot approach typically requires large (>75 ppm) changes in the observed CO_2 mixing ratio (Pataki et al., 2003b). At remote sites, the CO_2 variability is much smaller, resulting in much more severe requirements regarding measurement stability, precision and number of data

ACPD
10, 24563–24593, 2010

points. These requirements can be met by the employed laser spectrometer, because its high temporal resolution results in a sufficiently large sample size per event to accurately capture the tiny changes in the atmospheric CO_2 and provide a more robust estimate for the intercept value.

The average $\delta^{13}C_s$ signature of the regional pollution sources was calculated based on the above mentioned two-component mixing method. In Fig. 5, the correlation of the measured $\delta^{13}C$ and the inverse of CO_2 mixing ratio is individually shown for each event. The data points are one hour aggregates of the measured quantities recorded at one second temporal resolution. As such, they are not single-point measurements, but rather contain the continuous information of the whole averaging period. The intercept values range between −27 and −30‰, while the averaged value for the whole time-series in February 2009 was -28.3 ± 0.2‰, ($r^2 = 0.91$). They agree well with existing isotope ratio measurements of tropospheric CO_2 above Europe from aircraft sampling (Friedli et al., 1987; Zahn et al., 2000; Levin et al., 2002; Assonov et al., 2010). Furthermore, the mean value for fossil fuel in the 1990's was about −28.4‰, (Andres et al., 2000) and is expected to have changed little, due to the insignificant changes in the fossil emission rates.

The low $\delta^{13}C_s$ values during all events are consistent with combustion sources. $\delta^{13}C$ values reported for different combustion sources are on the order of −24‰, for coal, −30‰, to −26‰, for oil, −44‰, for natural gas and −27‰, to −22‰, for combustion of wood (Ciais et al., 1995; Andres et al., 1999; Schulze et al., 2004). The low values of events II, III and IV thus suggest a major contribution from oil combustion while the higher value of event I would again (see Fig. 4) be consistent with a substantial contribution from coal or biomass/wood burning.

While the measured carbon isotope data resulted in plausible estimates for anthropogenic CO_2 sources, the oxygen isotope of the atmospheric CO_2 is influenced by complex interactions involving both biotic and abiotic processes. Moreover, the equilibration process between oxygen isotopes of atmospheric CO_2 and of water proceeds without any net flux of CO_2 and depends on many meteorological variables (Francey

ACPD
10, 24563–24593, 2010

and Tans, 1987; Farquhar et al., 1993; Ciais et al., 1997). During winter, when the photosynthetic contribution (i.e. the amount of CO_2 isotopically exchanged with leaf water) can be neglected, all the remaining sources, which are primarily due to interaction with soils and release of anthropogenic CO_2, tend to deplete atmospheric CO_2 in ^{18}O, and $\delta^{18}O$ source signatures of −23‰ are readily possible (Miller et al., 1999). Although, the $\delta^{18}O$ follows a Keeling relation, the signatures of the "sources" determined from the linear regression are as low as −36‰. Even though similar low $\delta^{18}O$-values (−34‰) occurring in wintertime were measured by IRMS in Bern, Switzerland (Sturm et al., 2006), they cannot be interpreted as the oxygen isotopic composition of CO_2 released by any known source. These values reflect the limitation of the two source mixing assumption for $\delta^{18}O$, due to the effect of oxygen isotopic exchange without concentration changes. In this case, the Keeling relation can only give the $\delta^{18}O$ signature of an apparent instead of a real source.

The challenge then becomes to estimate the amount of CO_2 that was involved in oxygen isotopic exchange with soil water. As suggested by Tans (1998), in areas of low biological productivity a back-diffusion flux of CO_2 may become the major influence on $\delta^{18}O$ of atmospheric CO_2. According to this, a certain amount of CO_2 enters the soil from the air, equilibrates with soil water and leaves the soil again through diffusion. This process, also called invasion, is not associated with any net flux of CO_2 in or out of the soil. The $\delta^{18}O_s$ of CO_2 released by soils is mainly dependent on the oxygen isotope composition of soil water which approximately matches that of ground water. Thus, we are able not only to explain our results, but also make a quantitative estimate for the amount of invasion CO_2 required to match the observations. For this, we need first the $\delta^{18}O$ in soil water at regional scale. A mean value for the ^{18}O isotope distribution in soil water can be provided by the correlation between the seasonal evolution of $\delta^{18}O$ in precipitation and air temperature. In fact, the $\delta^{18}O$ value (in VSMOW (Vienna Standard Mean Ocean Water)) can be estimated from a linear regression (Rozanski et al., 1982, 1992; Schürch et al., 2003)

$$\delta^{18}O = 0.59\,T(°C) - 14.3 \quad (1)$$

ACPD
10, 24563–24593, 2010

of air temperature. Moreover, the temperature dependent value for the equilibrium fractionation factor ε_{eq} between the oxygen in CO_2 and water is given by (Brenninkmeijer et al., 1983)

$$\varepsilon_{eq} = 17\,604/T(\mathrm{K}) - 17.93 \quad (2)$$

By taking an average ambient temperature of 0 °C, the $^{18}O/^{16}O$ isotope ratio of soil water is given by Eq. (1) as −14.3‰, versus VSMOW or −53.6‰, versus VPDB-CO_2. Similarly, the fractionation factor for isotopically exchanged CO_2 is determined from Eq. (2) to be +46.6‰, versus VPDB-CO_2. When this CO_2 diffuses out of the soil, it undergoes a kinetic isotope fractionation with a maximum value of −8.7‰, but the disequilibrium between CO_2 and water near the surface results in a effective global mean fractionation value of about −7.2‰, (Miller et al., 1999). Hence, the signature of the back-diffused CO_2 ($\delta^{18}O_{inv}$) is about −14.2‰, which is more negative than the atmospheric air. Very similar results (−15‰) were reported earlier by Hesterberg and Siegenthaler (1991) for soil air samples. The obtained low $\delta^{18}O_s$ values of the Keeling plot can readily be explained by assuming certain amounts of invasion CO_2 admixed in the atmospheric background air with $\delta^{18}O_{bkg} \approx 0$‰. The amount of invasion CO_2 (C_{inv}) can be estimated using a simple isotopic mass balance calculation

$$\delta^{18}O_m C_m = \delta^{18}O_{bkg} C_{bkg} + \delta^{18}O_f C_f + \delta^{18}O_{inv} C_{inv} \quad (3)$$

where C_m, C_{bkg}, C_f and C_{inv} are the measured, background, fossil-derived and invasion CO_2 mixing ratios. By making the plausible assumption that the measured CO_2 mixing ratio increase is merely due to anthropogenic pollution caused by fossil fuel burning (i.e. $C_f = \Delta CO_2$) with a $\delta^{18}O_f$ value similar to the theoretical value for the oxygen isotope ratio of combustion of −17‰, (Kroopnick and Craig, 1972), the only unknown parameter in Eq. (3) is C_{inv}. Substituting the values for the other parameters results in C_{inv} peak values of about 16 ppm for the pollution events I and II, while for event III the amount is about 28 ppm. As one might expect, the amount of C_{inv} can differ from case to case depending on meteorological factors and soil conditions which influence

ACPD
10, 24563–24593, 2010

the time available for atmospheric CO_2 to diffuse into the soil, react, and equilibrate isotopically with soil water. Ultimately, the C_{inv} should be related to the amount of time that the air masses have been spend in the proximity of the ground before reaching JFJ. This hypothesis will be discussed based on the results of the next Section.

3.3 Backward LPDM calculations as source region identifier

Backward Lagrangian particle dispersion modeling is a powerful tool to identify the origin and transport pathways of the air arriving at a receptor site and thus efficiently complements the data analysis presented so far. As shown above, events II, III and IV have very similar $\delta^{13}C_s$ and CO:CO_2 ratio values and will thus be discussed first. The surface footprint for event II (Fig. 7b) indicates transport from south and southeast to JFJ over the highly industrialized Po Valley in Northern Italy. Pollutants from this region were entrained into the boundary layer and later transported in a South foehn episode to JFJ. Foehn is an airflow that only develops in mountainous regions and it is an effective mechanism for rapid vertical transport and mixing of boundary layer air. For event III the air masses were arriving at JFJ from the North-West during a short North foehn episode (Fig. 7c). Surface contact was indicated over western Switzerland, eastern France and the Benelux region. This is in excellent agreement with the observed CO_2 characteristics: a large increase in the mixing ratio which strongly correlates with the CO resulting in a CO:CO_2 ratio close to that of road transportation, and having a depleted ^{13}C content of −30‰, (as determined from the Keeling plot approach, Fig. 5), common to fossil fuel burning (diesel and/or gasoline). In the case of event IV, one would expect a "pure" combustion process from the CO vs. CO_2 relation. This is further supported by the intercept value ($\delta^{13}C_s$) on the Keeling plot. However, the rather small CO_2 mixing ratio changes and the accentuated spread in the $\delta^{13}C$-values make an accurate intercept determination difficult. Nevertheless, the surface footprint (Fig. 7d) shows that the air-masses mainly had surface contact over Eastern France, Belgium and to a smaller degree over western Germany. The general weather situation during this period was cold air advection from the north in which small convective precipitation

ACPD
10, 24563–24593, 2010

system were embedded that enabled vertical transport of air from surface emissions.

Event I was triggered by a South foehn, similarly to event II. However, the surface footprint for this episode (see Fig. 7a) indicates a very localized source area at the southern foot of the western Alps rather than covering the whole Po Valley. More spread out surface sensitivity was observed for the less polluted central and southern Italy and the adjacent maritime regions. The area of strong emission sensitivity corresponds to the upper Valais region in Switzerland and the Osalla valley in Italy. In winter time, residential wood burning for heating purposes is common in these Alpine valleys, especially in the villages, and has a dominant impact on air pollution (Szidat et al., 2007; Saurer et al., 2009; Perron et al., 2010). The wood burning as origin for the CO_2 fits very well with the observations: the steep CO:CO_2 slope (0.013) and the $\delta^{13}C$ Keeling plot intercept (−27.4‰).

Finally, in addition to the localization of potential source regions, LPDM calculations can also be used to estimate the total residence time of the air-masses close to the ground and relate them to the hypothesis of CO_2 invasion process discussed above. In fact, the calculated residence time in the boundary layer (Fig. 8) is qualitatively consistent with the estimated amount of CO_2 which went through the invasion process. As expected, longer residence times resulted in enhanced invasion. The averaged value of CO_2 interacting with soil for the whole period of February 2009 was estimated to 8.5 ± 5.4 ppm, which represents about 2% of the atmospheric CO_2. In the case of longer residence time of the air-masses close to the ground, the amount of CO_2 interacting with soil can be as high as 15–30 ppm CO_2, or 4–8% of atmospheric CO_2. This is consistent with values from literature, where the amount of atmospheric CO_2 that globally undergoes such invasion was estimated to be larger than the current annual fossil fuel combustion, i.e. 6 GtC yr^{-1} (Stern et al., 2001). Tans (1998) estimated a global CO_2 invasion of roughly 20% of the atmospheric column, while Cuntz et al. (2003) calculated a global CO_2 invasion flux of 18.6 GtC yr^{-1} with a global 3-D model of ^{18}O-CO_2.

ACPD
10, 24563–24593, 2010

4 Conclusions

This paper is the first demonstration of long-term, in situ and high precision isotope measurements of CO_2 under free tropospheric conditions at a high altitude site by laser absorption spectroscopy. The instrument has been operating unattended in the field and providing continuous, high temporal resolution measurements of $^{12}CO_2$, $^{13}CO_2$ and $^{16}O^{12}C^{18}O$. The advantage of continuous data is well illustrated by the presented one month measurement period with distinct pollution events. Considerable temporal variation in the isotopic composition of atmospheric CO_2, even during the course of a single day were successfully recorded. Capturing this variation with flask sampling and mass spectrometry would be impractical. Furthermore, the high temporal resolution of the QCLAS led to well constrained $\delta^{13}C_s$ values for regional emission sources. The combination of four different types of information, i.e. CO:CO_2 correlation, the $\delta^{13}C_s$ and $\delta^{18}O_s$ signatures determined by the Keeling plot approach and LPDM calculations, allowed for a consistent identification, characterization and spatial attribution of four distinct pollution events. We were able to explain the observed variations in the atmospheric CO_2mixing ratio by anthropogenic emissions with major contribution from fossil-fuel burning related to traffic, road-transport and heating, as well as wood burning for residential heating purposes. Air masses polluted with combustion derived CO_2 arriving at Jungfraujoch originated mainly from northern Italy, eastern France, Benelux region and southern Germany, as well as from the local Alpine Valleys of southern Switzerland. In addition, our data revealed that $\delta^{18}O$, despite its complex nature, is a promising tool to assess the oxygen isotope exchange between atmospheric CO_2 and soil H_2O. We suggest that the measured atmospheric $\delta^{18}O$ values are strongly influenced by the invasion process and, therefore, the apparent $\delta^{18}O_s$ signatures may be used for experimental quantification of this effect at regional scales. The invasion hypothesis is supported by two factors: i) the estimated amount of CO_2 interacting with soil is consistent with values from the literature, and ii) the expected dependence on the residence time of the air-masses above ground is confirmed by independent calculations based on a particle dispersion model.

ACPD
10, 24563–24593, 2010

The one month high precision measurements presented in this paper illustrates the reliability of the employed spectroscopic technique and the potential of such time series. More extended analysis of several years of data will, however, be necessary to capture interannual and seasonal variations of atmospheric CO_2, and to obtain more robust statistics for the characterization of various regional CO_2 sources.

Acknowledgements. We thank the International Foundation High Altitude Research Station Jungfraujoch and Gornergrat (HFSJG) for access to JFJ facilities and on-site support. Funding was provided by the Swiss NCCR-Quantum Photonics, the Swiss Federal Office for the Environment (FOEN) and the Swiss National Science Foundation. Calibration gases were analyzed within the Transnational Access (TA1) activity of the IMECC (Infrastructure for Measurements of the European Carbon Cycle) project.

References

Andreae, M. O. and Merlet, P.: Emission of trace gases and aerosols from biomass burning, Global Biogeochem Cy, 15, 955–966, doi:10.1029/2000GB001382, 2001. 24573

Andres, R. J., Fielding, D. J., Marland, G., Boden, T. A., Kumar, N., and Kearney, A. T.: Carbon dioxide emissions from fossil-fuel use, 1751–1950, Tellus B, 51, 759–765, doi:10.1034/j.1600-0889.1999.t01-3-00002.x, 1999. 24564, 24574

Andres, R. J., Marland, G., Boden, T., and Bischof, S.: Carbon dioxide emissions from fossil fuel consumption and cement manufacture, 1751–1991, and an estimate of their isotopic composition and latitudinal distribution, edited by: The Carbon Cycle, Wigley, T. M. L. and Schimel, D. S., Cambridge University Press, Cambridge, 2000. 24574

Archer, D., Eby, M., Brovkin, V., Ridgwell, A., Cao, L., Mikolajewicz, U., Caldeira, K., Matsumoto, K., Munhoven, G., Montenegro, A., and Tokos, K.: Atmospheric lifetime of fossil fuel carbon dioxide, Annu. Rev. Earth Pl. Sc., 37, 117–134, doi:10.1146/annurev.earth.031208.100206, 2009. 24564

Assonov, S. S., Brenninkmeijer, C. A. M., Schuck, T. J., and Taylor, P.: Analysis of ^{13}C and ^{18}O isotope data of CO_2 in CARIBIC aircraft samples as tracers of upper troposphere/lower stratosphere mixing and the global carbon cycle, Atmos. Chem. Phys., 10, 8575–8599, doi:10.5194/acp-10-8575-2010, 2010. 24574

Balzani Lööv, J. M., Henne, S., Legreid, G., Staehelin, J., Reimann, S., Prévôt, A. S. H., Steinbacher, M., and Vollmer, M. K.: Estimation of background concentrations of trace gases

ACPD
10, 24563–24593, 2010

at the Swiss Alpine site Jungfraujoch (3580 m asl), J. Geophys. Res., 113, 1–17, doi:10.1029/2007JD009751, 2008. 24566

Brenninkmeijer, C. A. M., Kraft, P., and Mook, W. G.: Oxygen isotope fractionation between CO_2 and H_2O, Isot. Geosci., 1, 181–190, doi:10.1016/S0009-2541(83)80015-1, 1983. 24576

Ciais, P., Tans, P. P., White, J. W. C., Trolier, M., Francey, R. J., Berry, J. A., Randall, D. R., Sellers, P. J., Collatz, G. J., and Schimel, D. S.: Partitioning of ocean and land uptake of CO_2 as inferred by $\delta^{13}C$ measurements from the NOAA Climate Monitoring and Diagnostics Laboratory Global Air Sampling Network, J. Geophys. Res., 100, 5051–5070, doi:10.1029/94JD02847, 1995. 24565, 24574

Ciais, P., Denning, A. S., Tans, P. P., Berry, J. A., Randall, D. A., Collatz, G. J., Sellers, P. J., White, J. W. C., Trolier, M., Meijer, H. A. J., Francey, R. J., Monfray, P., and Heimann, M.: A three-dimensional synthesis study of $\delta^{18}O$ in atmospheric CO_2 1. Surface fluxes, J. Geophys. Res., 102, 5857–5872, doi:10.1029/96JD02360, 1997. 24565, 24575

Conway, T. J., Tans, P. P., Waterman, L. S., Thoning, K. W., Kitzis, D. R., Masarie, K., and Zhang, N.: Evidence for interannual variability of the carbon cycle from the National Oceanic and Atmospheric Administration/Climate Monitoring and Diagnostics Laboratory Global Air Sampling Network, J. Geophys. Res., 99, 22831–22855, doi:10.1029/94JD01951, 1994. 24564

Cuntz, M., Ciais, P., Hoffmann, G., Allison, C. E., Francey, R. J., Knorr, W., Tans, P. P., White, J. W. C., and Levin, I.: A comprehensive global three-dimensional model of $\delta^{18}O$ in atmospheric CO_2: 2. Mapping the atmospheric signal, J. Geophys. Res., 108(D17), 4528, doi:10.1029/2002JD003154, 2003. 24565, 24578

Duncan, B. N., Logan, J. A., Bey, I., Megretskaia, I. A., Yantosca, R. M., Novelli, P. C., Jones, N. B., and Rinsland, C. P.: Global budget of CO, 1988–1997: Source estimates and validation with a global model, J. Geophys. Res., 112, D22301, doi:10.1029/2007JD008459, 2007. 24572

Farquhar, G. D., Lloyd, J., Taylor, J. A., Flanagan, L. B., Syvertsen, J. P., Hubick, K. T., Wong, S. C., and Ehleringer, J. R.: Vegetation effects on the isotope composition of oxygen in atmospheric CO_2, Nature, 363, 439–443, doi:10.1038/363439a0, 1993. 24575

Forrer, J., Rüttimann, R., Schneiter, D., Fischer, A., Buchmann, B., and Hofer, P.: Variability of trace gases at the high-Alpine site Jungfraujoch caused by meteorological transport processes, J. Geophys. Res., 105, 12241–12251, doi:10.1029/1999JD901178, 2000. 24566

Francey, R. J. and Tans, P. P.: Latitudinal variation in oxygen-18 of atmospheric CO_2, Nature, 327, 495–497, doi:10.1038/327495a0, 1987. 24565, 24574

ACPD
10, 24563–24593, 2010

Francey, R. J., Tans, P. P., Allison, C. E., Enting, I. G., White, J. W. C., and Trolier, M.: Changes in oceanic and terrestrial carbon uptake since 1982, Nature, 373, 326–330, doi:10.1038/373326a0, 1995. 24564

Friedli, H., Siegenthaler, U., Rauber, D., and Oeschger, H.: Measurements of concentration, $^{13}C/^{12}C$ and $^{18}O/^{16}O$ ratios of tropospheric carbon dioxide over Switzerland, Tellus B, 39, 80–88, doi:10.1111/j.1600-0889.1987.tb00272.x, 1987. 24574

Gamnitzer, U., Karstens, U., Kromer, B., Neubert, R. E. M., Meijer, H. A. J., Schroeder, H., and Levin, I.: Carbon monoxide: A quantitative tracer for fossil fuel CO_2?, J. Geophys. Res., 111, 1–19, doi:10.1029/2005JD006966, 2006. 24572

Ghosh, P. and Brand, W. A.: Stable isotope ratio mass spectrometry in global climate change research, Int. J. Mass Spectrom., 228, 1–33, doi:10.1016/S1387-3806(03)00289-6, 2003. 24569

Hesterberg, R. and Siegenthaler, U.: Production and stable isotopic composition of CO_2 in a soil near Bern, Switzerland, Tellus B, 43, 197–205, doi:10.1034/j.1600-0889.1991.00013.x, 1991. 24576

Kammer, A., Tuzson, B., Emmenegger, L., Knohl, A., Mohn, J., and Hagedorn, F.: Application of a quantum cascade laser-based spectrometer in a closed chamber system for real-time $\delta^{13}C$ and $\delta^{18}O$ measurements of soil-respired CO_2, Agric. Forest Meteorol., doi:10.1016/j.agrformet.2010.09.001, press, 2010. 24567

Keeling, C. D.: The concentration and isotopic abundances of atmospheric carbon dioxide in rural areas, Geochim. Cosmochim. Ac., 13, 322–334, 1958. 24573

Keeling, C. D., Whorf, T. P., Wahlen, M., and Plicht, J.: Interannual extremes in the rate of rise of atmospheric carbon dioxide since 1980, Nature, 375, 666–670, doi:10.1038/375666a0, 1995. 24564

Kroopnick, P. and Craig, H.: Atmospheric oxygen: isotopic composition and solubility fractionation, Science, 175, 54–55, doi:10.1126/science.175.4017.54, 1972. 24565, 24576

Levin, I. and Karstens, U.: Inferring high-resolution fossil fuel CO_2 records at continental sites from combined $^{14}CO_2$ and CO observations, Tellus B, 59, 245–250, doi:10.1111/j.1600-0889.2006.00244.x, 2007. 24572

Levin, I., Ciais, P., Langenfelds, R., Schmidt, M., Ramonet, M., Sidorov, K., Tchebakova, N., Gloor, M., Heimann, M., Schulze, E. D., Vygodskaya, N. N., Shibistova, O., and Lloyd, J.: Three years of trace gas observations over the EuroSiberian domain derived from aircraft sampling - A concerted action, Tellus B, 54, 696–712, doi:10.1034/j.1600-0889.2002.01352.

ACPD
10, 24563–24593, 2010

x, 2002. 24574
Miller, J. B., Yakir, D., White, J. W. C., and Tans, P. P.: Measurement of $^{18}O/^{16}O$ in the soil-atmosphere CO_2 flux, Global Biogeochem. Cy., 13, 761–774, doi:10.1029/1999GB900028, 1999. 24575, 24576
Nelson, D. D., McManus, J. B., Herndon, S. C., Zahniser, M. S., Tuzson, B., and Emmenegger, L.: New method for isotopic ratio measurements of atmospheric carbon dioxide using a 4.3 μm pulsed quantum cascade laser, Appl. Phys. B-Lasers O., 90, 301–309, doi:10.1007/s00340-007-2894-1, 2008. 24566
Pataki, D. E., Bowling, D. R., and Ehleringer, J. R.: Seasonal cycle of carbon dioxide and its isotopic composition in an urban atmosphere: Anthropogenic and biogenic effects, J. Geophys. Res., 108, 4735–4743, doi:10.1029/2003JD003865, 2003a. 24565
Pataki, D. E., Ehleringer, J. R., Flanagan, L. B., Yakir, D., Bowling, D. R., Still, C., Buchmann, N., Kaplan, J. O., and Berry, J. A.: The application and interpretation of Keeling plots in terrestrial carbon cycle research, Global Biogeochem. Cy., 17, 1022–1036, doi:10.1029/2001GB001850, 2003b. 24573
Perron, N., Sandradewi, J., Alfarra, M. R., Lienemann, P., Gehrig, R., Kasper-Giebl, A., Lanz, V. A., Szidat, S., Ruff, M., Fahrni, S., Wacker, L., Baltensperger, U., and Prévôt, A. S. H.: Composition and sources of particulate matter in an industrialised Alpine valley, Atmos. Chem. Phys. Discuss., 10, 9391–9430, doi:10.5194/acpd-10-9391-2010, 2010. 24578
Randerson, J. T., Thompson, M. V., Conway, T. J., Fung, I. Y., and Field, C. B.: The contribution of terrestrial sources and sinks to trends in the seasonal cycle of atmospheric carbon dioxide, Global Biogeochem. Cy., 11, 535–560, doi:10.1029/97GB02268, 1997. 24564
Rozanski, K., Sonntag, C., and Münnich, K. O.: Factors controlling stable isotope composition of European precipitation, Tellus B, 34, 142–150, doi:10.1111/j.2153-3490.1982.tb01801.x, 1982. 24575
Rozanski, K., Araguás-Araguás, L., and Gonfiantini, R.: Relation between long-term trends of oxygen-18 isotope composition of precipitation and climate, Science, 258, 981–985, doi:10.1126/science.258.5084.981, 1992. 24575
Saurer, M., Prévôt, A. S. H., Dommen, J., Sandradewi, J., Baltensperger, U., and Siegwolf, R. T. W.: The influence of traffic and wood combustion on the stable isotopic composition of carbon monoxide, Atmos. Chem. Phys., 9, 3147–3161, doi:10.5194/acp-9-3147-2009, 2009. 24578
Schulze, B., Wirth, C., Linke, P., Brand, W., Kuhlmann, I., Horna, V., and Schulze, E. D.: Laser

ACPD
10, 24563–24593, 2010

ablation-combustion-GC-IRMS – A new method for online analysis of intra-annual variation of $\delta^{13}C$ in tree rings, Tree Physiol., 24, 1193–1201, 2004. 24574
Schürch, M., Kozel, R., Schotterer, U., and Tripet, J. P.: Observation of isotopes in the water cycle – The Swiss National Network (NISOT), Environ. Geol., 45, 1–11, doi:10.1007/s00254-003-0843-9, 2003. 24575
Seibert, P. and Frank, A.: Source-receptor matrix calculation with a Lagrangian particle dispersion model in backward mode, Atmos. Chem. Phys., 4, 51–63, doi:10.5194/acp-4-51-2004, 2004. 24569, 24570
Stern, L. A., Amundson, R., and Baisden, W. T.: Influence of soils on oxygen isotope ratio of atmospheric CO_2, Global Biogeochem. Cy., 15, 753–759, doi:10.1029/2000GB001373, 2001. 24578
Stohl, A., Forster, C., Frank, A., Seibert, P., and Wotawa, G.: Technical note: The Lagrangian particle dispersion model FLEXPART version 6.2, Atmos. Chem. Phys., 5, 2461–2474, doi:10.5194/acp-5-2461-2005, 2005. 24569
Sturm, P., Leuenberger, M., Valentino, F. L., Lehmann, B., and Ihly, B.: Measurements of CO_2, its stable isotopes, O_2/N_2, and ^{222}Rn at Bern, Switzerland, Atmos. Chem. Phys., 6, 1991–2004, doi:10.5194/acp-6-1991-2006, 2006. 24575
Szidat, S., Prévôt, A. S. H., Sandradewi, J., Alfarra, M. R., Synal, H. A., Wacker, L., and Baltensperger, U.: Dominant impact of residential wood burning on particulate matter in Alpine valleys during winter, Geophys. Res. Lett., 34, L05820, doi:10.1029/2006GL028325, 2007. 24578
Tans, P. P.: Oxygen isotopic equilibrium between carbon dioxide and water in soils, Tellus B, 50, 163–178, doi:10.1034/j.1600-0889.1998.t01-1-00004.x, 1998. 24575, 24578
Tans, P. P., Conway, T. J., and Nakazawa, T.: Latitudinal Distribution of the Sources and Sinks of Atmospheric Carbon Dioxide Derived From Surface Observations and an Atmospheric Transport Model, J. Geophys. Res., 94, 5151–5172, doi:10.1029/JD094iD04p05151, 1989. 24564
Turnbull, J. C., Miller, J. B., Lehman, S. J., Tans, P. P., Sparks, R. J., and Southon, J.: Comparison of $^{14}CO_2$, CO, and SF_6 as tracers for recently added fossil fuel CO_2 in the atmosphere and implications for biological CO_2 exchange, Geophys. Res. Lett., 33, L01817, doi:10.1029/2005GL024213, 2006. 24572
Turnbull, J. C., Karion, A., Fischer, M. L., Faloona, I., Guilderson, T., Lehman, S. J., Miller, B. R., Miller, J. B., Montzka, S., Sherwood, T., Saripalli, S., Sweeney, C., and Tans, P. P.: Mea-

ACPD
10, 24563–24593, 2010

surement of fossil fuel derived carbon dioxide and other anthropogenic trace gases above Sacramento, California in Spring 2009, Atmos. Chem. Phys. Discuss., 10, 21567–21613, doi:10.5194/acpd-10-21567-2010, 2010. 24572

Tuzson, B., Mohn, J., Zeeman, M. J., Werner, R. A., Eugster, W., Zahniser, M. S., Nelson, D. D., McManus, J. B., and Emmenegger, L.: High precision and continuous field measurements of $\delta^{13}C$ and $\delta^{18}O$ in carbon dioxide with a cryogen-free QCLAS, Appl. Phys. B-Laser O., 92, 451–458, doi:10.1007/s00340-008-3085-4, 2008. 24566

Tuzson, B., Hiller, R. V., Zeyer, K., Eugster, W., Neftel, A., Ammann, C., and Emmenegger, L.: Field intercomparison of two optical analyzers for CH4 eddy covariance flux measurements, Atmos. Meas. Tech. Discuss., 3, 2961–2993, doi:10.5194/amtd-3-2961-2010, 2010. 24568

Vollmer, M. K., Juergens, N., Steinbacher, M., Reimann, S., Weilenmann, M., and Buchmann, B.: Road vehicle emissions of molecular hydrogen (H_2) from a tunnel study, Atmos. Environ., 41, 8355–8369, doi:10.1016/j.atmosenv.2007.06.037, 2007. 24573

Werle, P., Mücke, R., and Slemr, F.: The limits of signal averaging in atmospheric trace-gas monitoring by tunable diode-laser absorption spectroscopy (TDLAS), Appl. Phys. B-Laser O., 57, 131–139, doi:10.1007/BF00425997, 1993. 24567

Yakir, D. and Wang, X. F.: Fluxes of CO_2 and water between terrestrial vegetation and the atmosphere estimated from isotope measurements, Nature, 380, 515–517, doi:10.1038/380515a0, 1996. 24565

Zahn, A., Neubert, R., and Platt, U.: Fate of long-lived trace species near the Northern Hemispheric tropopause 2. Isotopic composition of carbon dioxide ($^{13}CO_2$, $^{14}CO_2$, and $C^{18}O^{16}O$), J. Geophys. Res., 105, 6719–6735, doi:10.1029/1999JD901000, 2000. 24574

Zeeman, M. J., Tuzson, B., Emmenegger, L., Knohl, A., Buchmann, N., and Eugster, W.: Conditional CO2 flux analysis of a managed grassland with the aid of stable isotopes, Biogeosciences Discuss., 6, 3481–3510, doi:10.5194/bgd-6-3481-2009, 2009. 24566

Zellweger, C., Hüglin, C., Klausen, J., Steinbacher, M., Vollmer, M., and Buchmann, B.: Intercomparison of four different carbon monoxide measurement techniques and evaluation of the long-term carbon monoxide time series of Jungfraujoch, Atmos. Chem. Phys., 9, 3491–3503, doi:10.5194/acp-9-3491-2009, 2009. 24572, 24573

Zondervan, A. and Meijer, H. A. J.: Isotopic characterisation of CO_2 sources during regional pollution events using isotopic and radiocarbon analysis, Tellus B, 48, 601–612, doi:10.1034/j.1600-0889.1996.00013.x, 1996. 24572

ACPD
10, 24563–24593, 2010

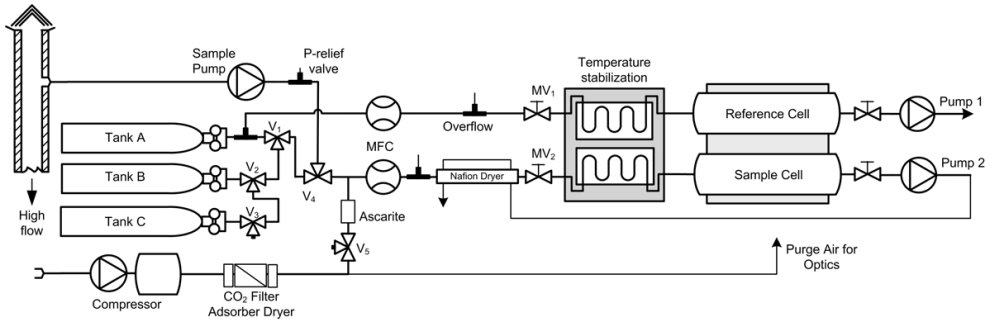

Fig. 1. Sampling setup of the QCLAS. V_i and MV_i are solenoid- and manual-valves, MFC-mass flow controller and Tank A, B, C are the calibration gases (see text for more details).

ACPD
10, 24563–24593, 2010

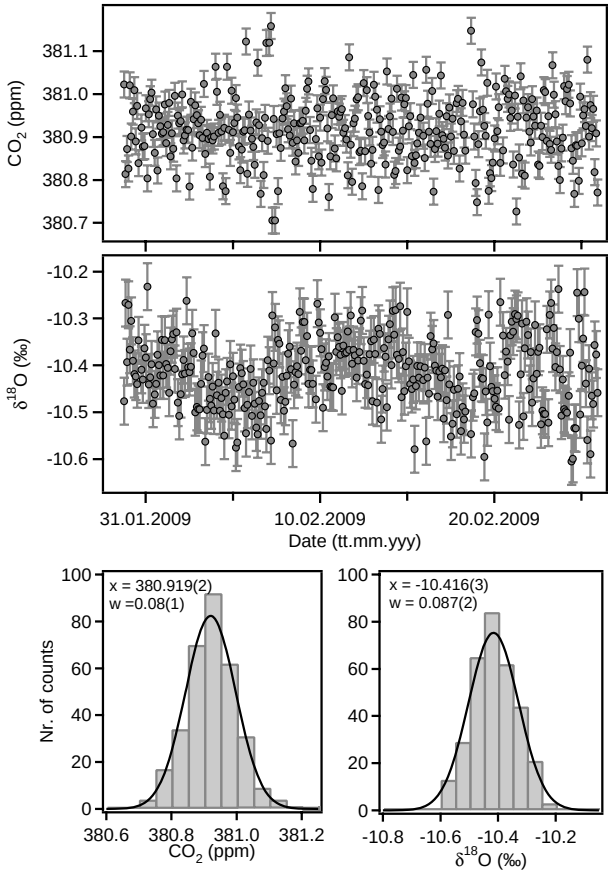

Fig. 2. Long term stability of the QCLAS. The data show repeated measurements of the secondary standard for February, 2009. The individual δ-values of each calibration step were plotted as a histogram with a 0.05‰, bin width.

ACPD
10, 24563–24593, 2010

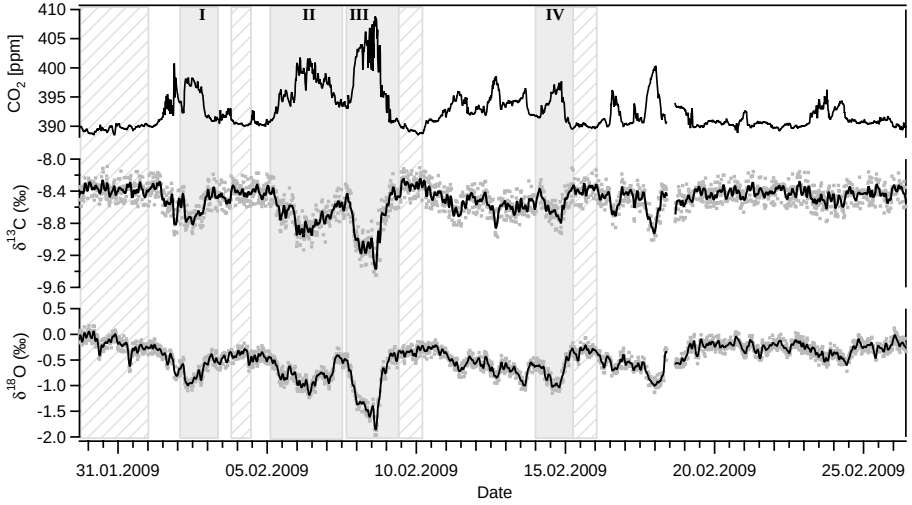

Fig. 3. Time series of tropospheric CO_2 mixing ratio and its isotopic composition. For the delta values, the gray dots represent 10 min averages, while the solid line is an interpolation through the data using a smooth cubic spline. The shaded areas indicate distinct pollution events, while periods with the free tropospheric background conditions are highlighted by hatched areas.

ACPD
10, 24563–24593, 2010

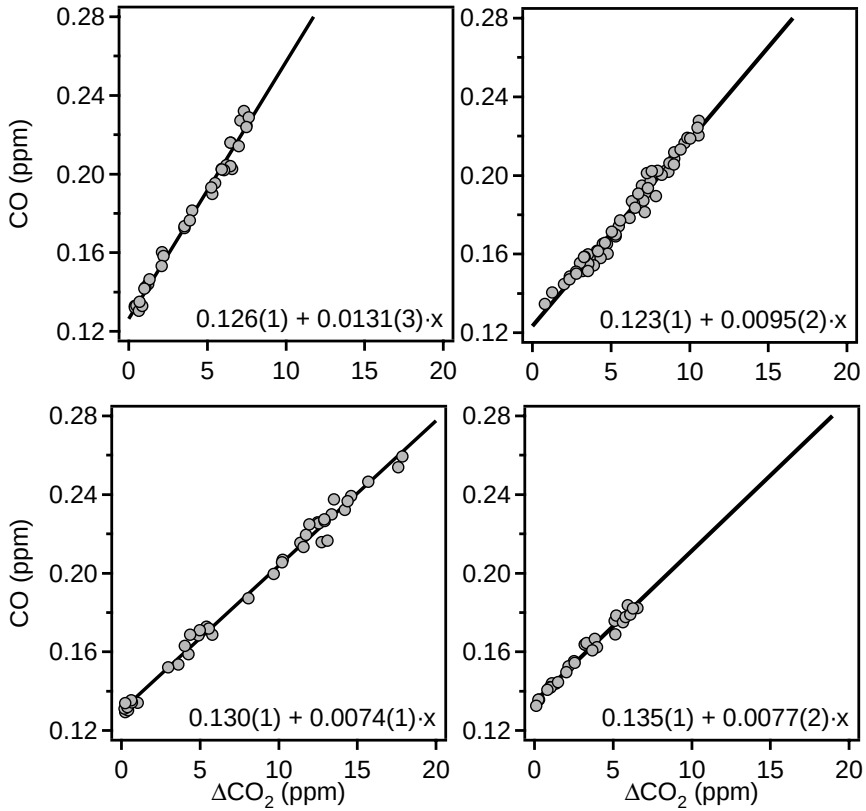

Fig. 4. Scatter plot of CO versus CO_2 above background (ΔCO_2) for the four selected pollution events. Linear fits and 1σ uncertainties (in parenthesis) are also given. Since absolute CO mixing ratios are used, the intercept of the regression corresponds to the continental background CO level. The slope is indicative for the combustion process with larger values representing poorer, i.e. less complete, combustion.

ACPD
10, 24563–24593, 2010

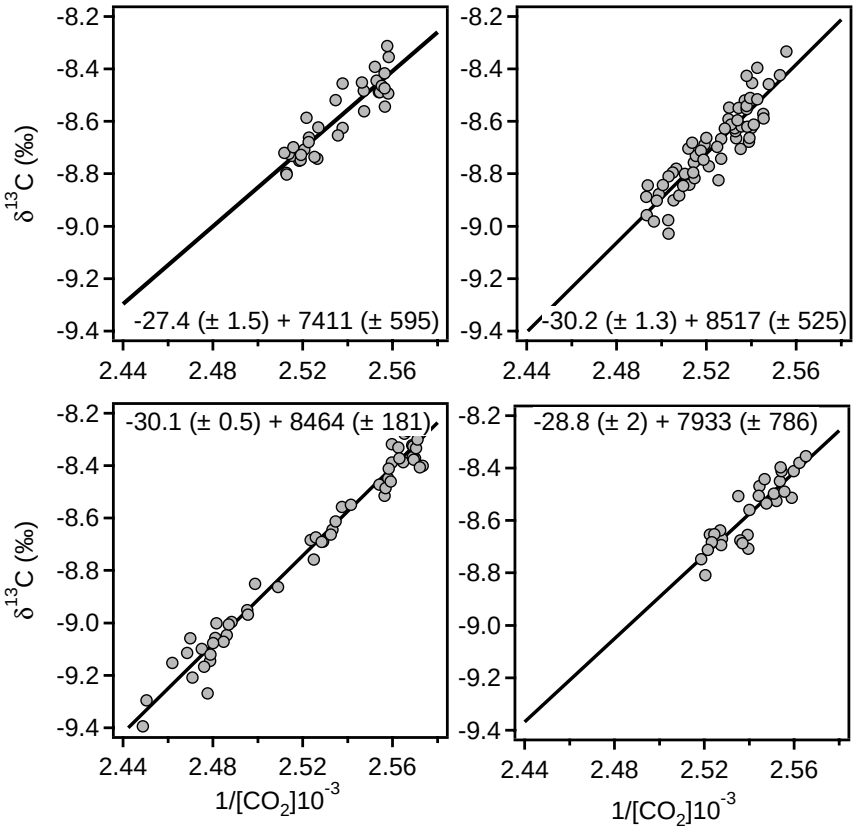

Fig. 5. Keeling plots for data collected during the individual pollution events. $\delta^{13}C$ values representing one hour aggregates are plotted against the inverse of CO_2 mixing ratio. The intercept and the slope of the ordinary least square linear regression is given together with their 1σ uncertainties.

ACPD
10, 24563–24593, 2010

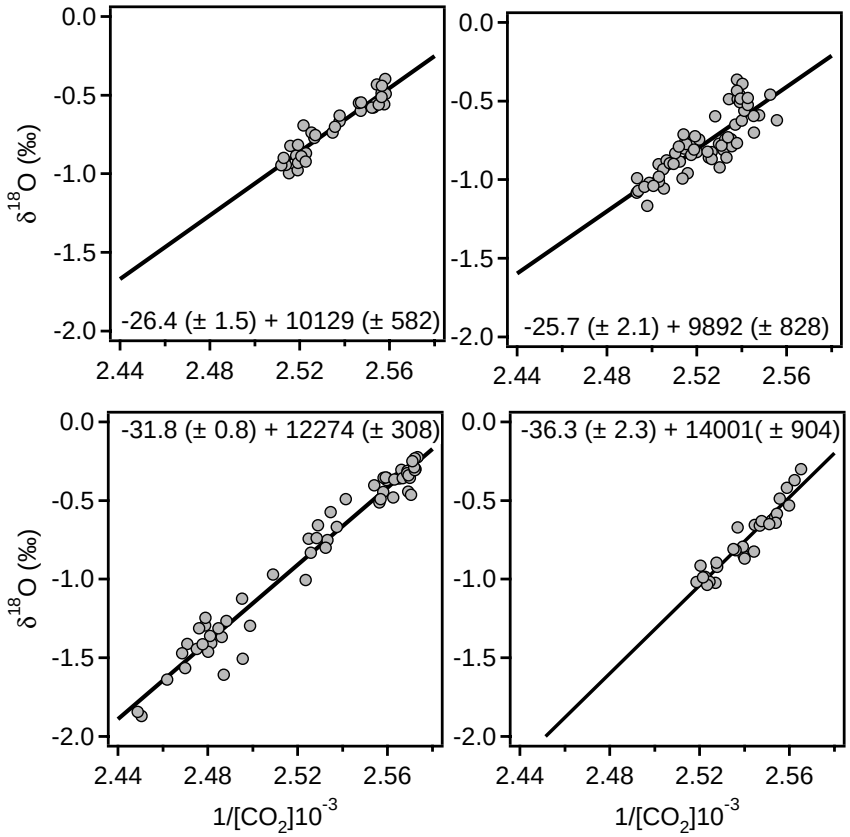

Fig. 6. Keeling plots for data collected during the individual pollution events. $\delta^{18}O$ values representing one hour aggregates are plotted against the inverse of CO_2 mixing ratio. The intercept and the slope of the ordinary least square linear regression is given together with their 1σ uncertainties.

ACPD
10, 24563–24593, 2010

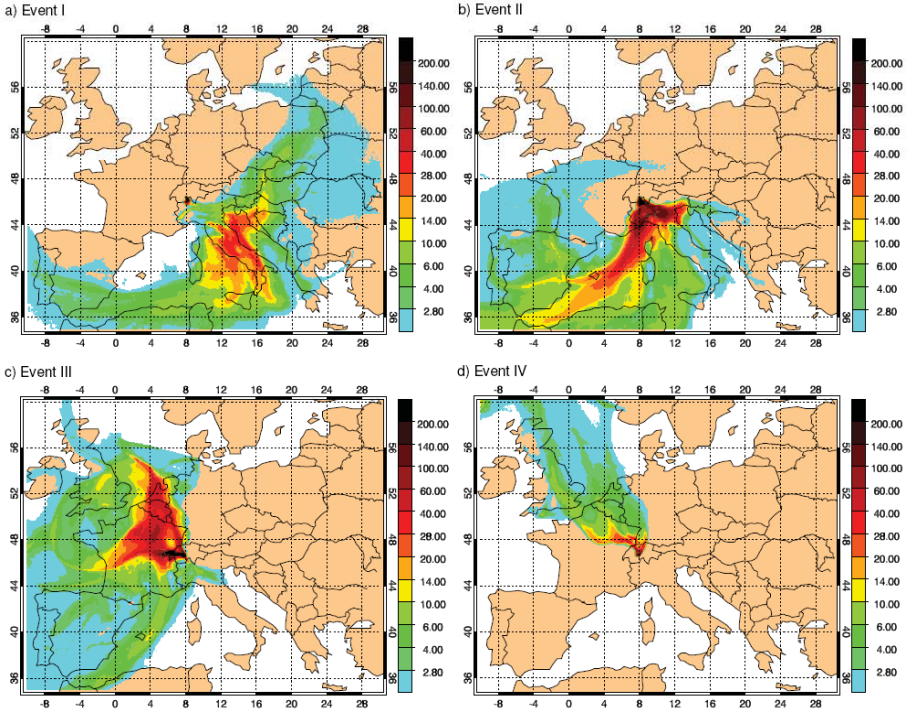

Fig. 7. Backward LPDM calculations, showing the potential source regions (surface footprints) of air-masses reaching JFJ during pollution events. Yellow to red colors ($s\,kg^{-1}\,m^3$) identify regions from which elevated CO_2 potentially originated.

ACPD
10, 24563–24593, 2010

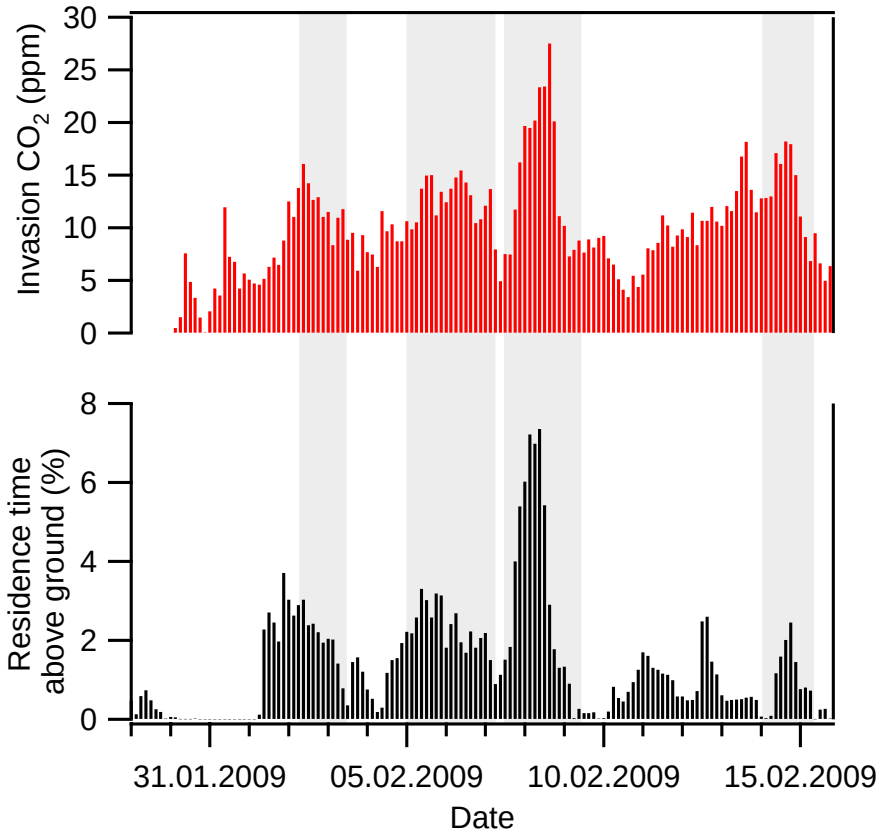

Fig. 8. Top panel indicates the amount of atmospheric CO_2 which exchanged its oxygen isotope with soil water (for details see text). Bottom panel shows the total residence time of the air-masses in a layer up to 100 m above ground relative to total residence time (5-days) as calculated from the LPDM at 4 h time intervals.

ACPD
10, 24563–24593, 2010